Article

Photocatalytic CO$_2$ Conversion Using Anodic TiO$_2$ Nanotube-Cu$_x$O Composites

Timofey P. Savchuk [1,2,3,*], Ekaterina V. Kytina [1], Elizaveta A. Konstantinova [1,*], Vladimir G. Kytin [1], Olga Pinchuk [2], Andrey K. Tarhanov [2], Vladimir B. Zaitsev [1] and Tomasz Maniecki [3]

[1] Physics Department M.V., Lomonosov Moscow State University, Leninskie Gory 1-2, 119991 Moscow, Russia
[2] Institute of Advanced Materials and Technologies, National Research University of Electronic Technology—MIET, Bld. 1, Shokin Square, Zelenograd, 124498 Moscow, Russia
[3] Institute of General and Ecological Chemistry, Lodz University of Technology, Zeromskiego 116, 90-924 Lodz, Poland
[*] Correspondence: wewillbe01@gmail.com (T.P.S.); liza35@mail.ru (E.A.K.)

Abstract: Nanosized titanium dioxide (TiO$_2$) is currently being actively studied by the global scientific community, since it has a number of properties that are important from a practical point of view. One of these properties is a large specific surface, which makes this material promising for use in photocatalysts, sensors, solar cells, etc. In this work, we prepared photocatalysts based on TiO$_2$ nanotubes for converting carbon dioxide (CO$_2$) into energy-intensive hydrocarbon compounds. Efficient gas-phase CO$_2$ conversion in the prepared single-walled TiO$_2$ nanotube-Cu$_x$O composites was investigated. Parameters of defects (radicals) in composites were studied. Methanol and methane were detected during the CO$_2$ photoreduction process. In single-walled TiO$_2$ nanotubes, only Ti^{3+}/oxygen vacancy defects were detected. The Cu^{2+} centers and O$_2^-$ radicals were found in TiO$_2$ nanotube-Cu$_x$O composites using the EPR technique. It has been established that copper oxide nanoparticles are present in the TiO$_2$ nanotube-Cu$_x$O composites in the form of the CuO phase. A phase transformation of CuO to Cu$_2$O takes place during illumination, as has been shown by EPR spectroscopy. It is shown that defects accumulate photoinduced charge carriers. The mechanism of methane and methanol formation is discussed. The results obtained are completely original and show high promise for the use of TiO$_2$-Cu$_x$O nanotube composites as photocatalysts for CO$_2$ conversion into hydrocarbon fuel precursors.

Keywords: TiO$_2$ nanotube-Cu$_x$O composites; CO$_2$ photocatalytic conversion; radical; EPR

1. Introduction

An increase in the concentration of atmospheric CO$_2$ is considered one of the main sources of irreversible and dangerous climate change [1,2]. Therefore, conversion of CO$_2$ into useful products is a globally important objective. Different approaches are being developed for CO$_2$ conversion [3]. One promising approach is photocatalytic reduction of CO$_2$ [4]. The issue is that most of the known photocatalysts are too inefficient [5]. Among others, photocatalysts based on nanostructured TiO$_2$ have such important advantages as chemical stability and photocorrosion resistance, and suitable electron energy spectrum [6,7]. TiO$_2$ is also non-toxic material. Titania nanotube arrays (TiO$_2$ NTs) have large specific surface area. Due to their geometry and surface structure, they can promote faster diffusion of photocatalytic reaction products, directional charge transfer, and lower recombination rates of photoinduced charge carriers in comparison to TiO$_2$ nanoparticles [8–10]. Highly ordered TiO$_2$ NTs arrays can be formed by electrochemical oxidation of Ti [6,11,12]. TiO$_2$ NTs formed electrochemically in ethylene-glycol-based electrolyte contain an inner layer (IL) enriched with organic products, and an outer layer (OL) of mostly pure TiO$_2$ [13,14]. To improve catalytic activity and obtain crystalline TiO$_2$ structure, as-formed TiO$_2$ NTs arrays are annealed in air. After annealing, the inner layer of a nanotube has a

mesoporous structure with a mixture of anatase and rutile nanocrystals with an average size of ~7 nm with the presence of carbon species [15,16]. The outer layer of a nanotube consists of practically stoichiometric anatase [15]. One of the issues of nanostructured TiO_2 catalysts is low absorption of visible light due to a wide band gap. Several ways have been proposed to improve the photocatalytic activity of TiO_2-based materials under visible-light illumination [6]. Creation of nano-heterojunctions with Cu_xO species is an effective method [17–23].

Photocatalytic reduction of CO_2 in water and alkaline solutions was shown in [24] using TiO_2-Cu_xO composites with different Cu content deposited onto a molecular sieve. It was demonstrated that these composites enhanced CO_2 photoreduction with selective formation of oxalic acid. Furthermore, methanol and acetic acid were observed on the molecular sieve combinate system. In [25], computational modeling and experimental studies were conducted to elucidate the role of Cu sites in promoting CO_2 reduction on TiO_2. The nanocomposites demonstrated significantly higher activity than bare TiO_2 in photocatalysis, and the activity was found to be related to the chemical state of surface Cu+ species. According to modeling studies, the highly dispersed Cu sites likely contributed to the improved photocatalysis by stabilizing surface adsorption of CO_2 on TiO_2. The experimental and modeling studies further confirmed the direct involvement of surface Cu sites in CO generation via CO_2 reduction. Additionally, using TiO_2-Cu_xO heterojunctions can promote photocatalytic decomposition reactions of phenol and acetone [26] and other organic compounds [27,28]. In [29], it was shown that an optimum CuO and TiO_2 ratio was necessary to achieve the highest efficiency of methanol conversion to methyl formate. In addition, in [30], the authors describe the TiO_2-protecting effect of Cu_2O from photocorrosion during CO_2 reduction in a saturated solution.

The review [31] has shown that, due to the smaller band gap of metal oxides, such as Cu_xO, the light absorption capacity of TiO_2 can be improved in heterojunctions. Methanol production was reported in CO_2 photoreduction process when TiO_2 is doped with CuO that provides the highest yield. Cu_2O is named in [31] as very promising and the most frequently used dopant candidate for the photoreduction of CO_2. It has a band gap ranging from 2 to 2.2 eV that absorbs visible light effectively.

From our point of view, the enhancement of photocatalytic activity in TiO_2-Cu_xO heterojunctions compared to nanostructured TiO_2 is due to effective absorption of visible light in Cu_xO nanoparticles, and charge separation at the heterojunction. The latter reduces the recombination rate of photoexcited electrons and holes.

Activity and selectivity of a TiO_2-Cu_xO catalyst depends on the method of its synthesis [17–23,32]. Moreover, the efficiency and selectivity of CO_2 conversion by TiO_2-Cu_xO catalysts varies during the conversion process [17–23,32]. One of the possible origins is the reduction of CuO to Cu_2O. Additionally, the properties of TiO_2-Cu_xO heterojunctions depend on the catalyst's microstructure. The efficiency of methanol production on TiO_2-NTs-Cu_xO photocatalysts with different sizes and compositions of copper oxide particles has been studied in [32]. The output of methanol was significantly different for catalysts with different x and size of Cu_xO particles. The results were explained by the dependence of electron energy spectrum on copper oxide phase composition and by the dependence of methanol production rate on the size, shape and distribution of Cu_xO particles [32].

To our knowledge, there is a very limited number of articles reporting the study of the photocatalytic activity of TiO_2 NTs arrays obtained in ethylene-glycol-based electrolyte and TiO_2 NTs-Cu_xO arrays in the CO_2 conversion process in a gas phase in the presence of water vapor [7,9,33]. Moreover, the effect of multilayered structures and the role of inner layers was not discussed much in these publications.

In our previous publication, in [34] we reported a comparative study of the photocatalytic properties of TiO_2 multi-walled and single-walled nanotube arrays for photoinduced CO_2 conversion in the gas phase, their structures and their defect properties. Electron paramagnetic resonance (EPR) spectroscopy was applied to observe the structural defects in the outer and inner layers of TiO_2 nanotubes and analyze their effect on the photocat-

alytic properties of the nanotubes [35]. The present work aims to study the structural, electronic and photocatalytic properties of TiO_2 NTs/Cu_xO composites obtained from TiO_2 NTs arrays without IL by Cu_xO deposition applying successive ionic layer adsorption and reaction (SILAR). This section may be divided by subheadings. It should provide a concise and precise description of the experimental results, their interpretation and conclusions that can be drawn.

2. Results and Discussion

2.1. Samples Morphology and Composition

Morphology of SW TiO_2 NTs/Cu_xO has been studied using a scanning electron microscope equipped with energy-dispersion X-ray spectroscopy. SEM images of investigated samples are presented in Figure 1.
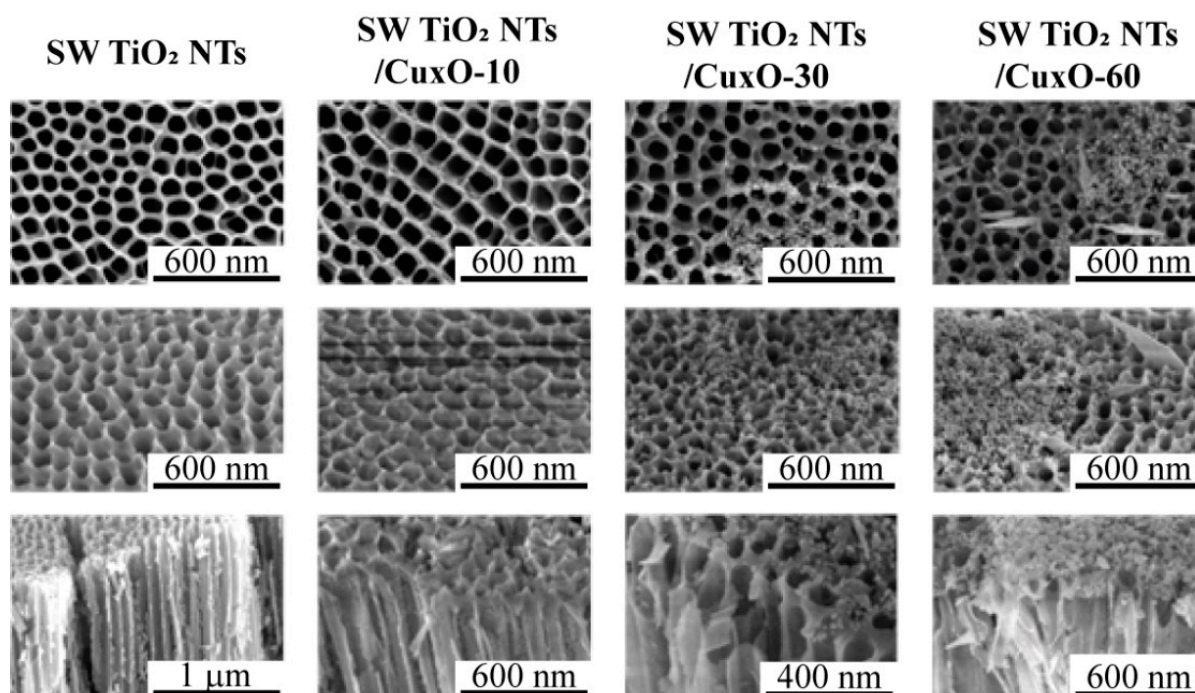

Figure 1. SEM images of SW TiO_2 NTs array surface before and after copper oxide Cu_xO deposition.

As can be seen from SEM images, the size of deposited Cu_xO particles increases with amount of deposition cycles. It is also noticeable that deposition in the described conditions leads to formation of islands and non-homogeneous coverage of the surface of SW TiO_2 NTs arrays by Cu_xO nanoparticles.

The size range of deposited nanoparticles were 9–21 nm, 11–36 nm and 14–40 nm for SW TiO_2 NTs/Cu_xO-10/30/60 samples, respectively. With an increase in the amount of deposition cycles, nanoparticles form agglomerates while the sizes of nanoparticles change slightly and do not depend significantly on the amount of cycles. A characteristic feature of the SW TiO_2 NTs/Cu_xO-60 sample is the presence of nanoparticles with the shape of needles or sheets with the length from 100 nm to 500 nm and 30 to 40 nm thickness. It is well noticeable that Cu_xO deposition inside the tube does not take place, i.e., only the top surfaces of the SW TiO_2 NTs arrays are modified during deposition.

As it is seen from the energy dispersive X-ray microanalysis (Table 1), the amount of copper at the SW TiO_2 NTs arrays' surface varies non-linearly depending on the amount of deposition cycles, and reaches about 3.3 at. % after 60 deposition cycles.

Table 1. EDX microanalysis data for SW TiO_2 NTs arrays with different copper content.

	SW TiO_2 NTs	SW TiO_2 NTs/ Cu_xO-10	SW TiO_2 NTs/ Cu_xO-30	SW TiO_2 NTs/ Cu_xO-60
Ti, at. %	31.9	32.9	34.0	31.4
O, at. %	55.7	58.1	56.6	58.5
F, at. %	0.3	0.7	0.0	0.4
C, at. %	4.4	6.4	3.8	6.0
Cu, at. %	0.0	2.2	3.0	3.3
Al, at. %	0.5	0.3	0.2	0.3

The obtained SW TiO_2 NTs and SW TiO_2 NTs/Cu_xO-60 samples were investigated by X-ray diffraction analysis (Figure S1). The copper oxide phase was not recorded by XRD, because of the amount of the $CuxO$ is too small to be registered by this method.

2.2. Optical Properties

The diffuse reflectance spectra depend on the amount of copper oxide, as presented in Figure 2.
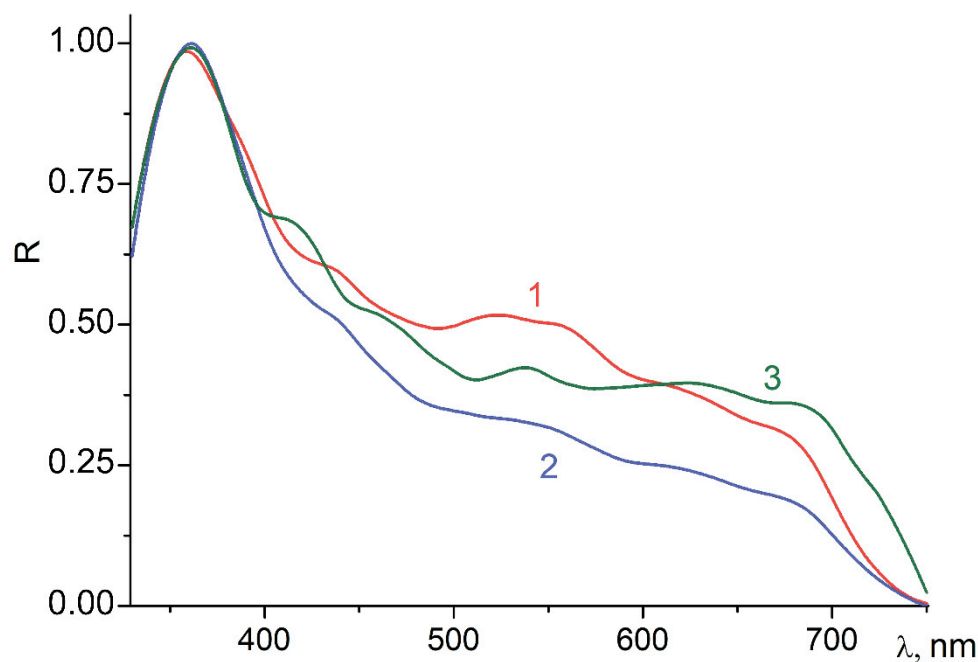
Figure 2. Normalized Spectra of Diffuse Reflection of Light from the SW TiO_2 NTs/Cu_xO-10 (1), SW TiO_2 NTs/Cu_xO-30 (2) and SW TiO_2 NTs/Cu_xO-60 (3).

According to calculations performed using the Kubelka-Munk theory, the optical band gap is similar for all samples under study: 3.1 ± 0.1 eV for SW TiO_2 NTs samples and 3.3 ± 0.1 eV for NTs/Cu_xO samples. All NTs/Cu_xO samples showed higher light absorption in visible areas compared to pure SW TiO_2 NTs. The samples of SW TiO_2 NTs/Cu_xO-30 possess the most efficient visible light absorption from all samples under study.

2.3. Photocatalytic Conversion of CO_2

Prepared samples were investigated in situ during CO_2 conversion in gas phase in the presence of water vapor. The products of photoelectrochemical reactions were detected by chromatograph equipped with a plasma ionization detector (PID). The outcome of reaction products was calculated per unit of specific surface area for each sample 7.7×10^{-3} m^2/cm^2. The specific surface area has been calculated in the frame of a simple geometric model using scanning electron microscopy data (Figure S2); the methodology was described in [34].

Three LEDs operating at 370 nm main wavelength were used for illumination. Illumination intensity at the sample was about 23 mW/cm^2. The measurement process was carried out in four stages: (1) pumping of helium through the reactor during 10 h; (2) cleaning of the sample surface from organic impurities in helium flux under LED illumination; (3) photoinduced conversion of CO_2 (helium flux replaced by CO_2 flux); (4) registration of relaxation after turning off illumination. Gas flux was set to 1.1 mL/min. Results are presented in Figure 3. Methane and methanol were detected as main reaction products. Acetaldehyde, ethanol, formic acid and acetone were detected in helium flux under illumination, but their amount did not increase after CO_2 supplement. The kinetics of acetaldehyde formation is presented in the Supplementary Material, Figure S3.
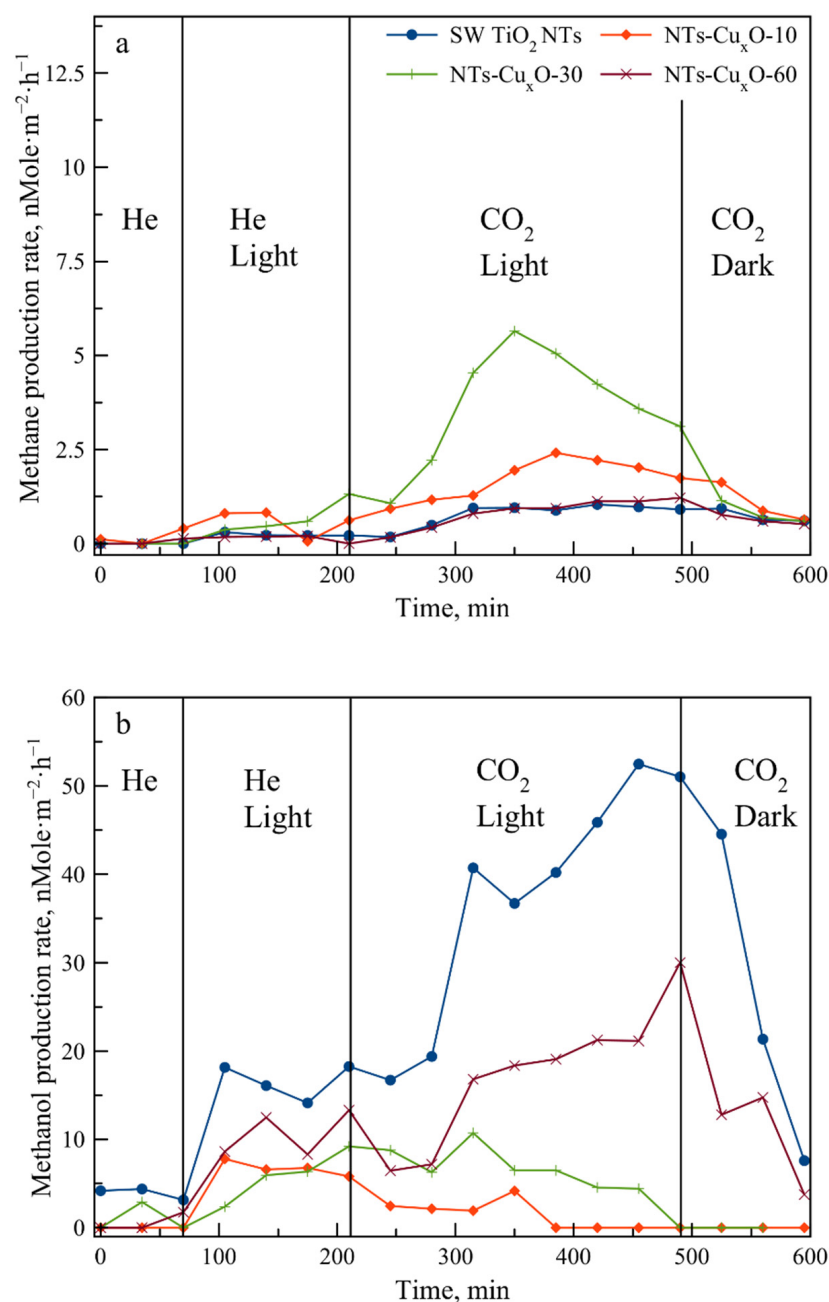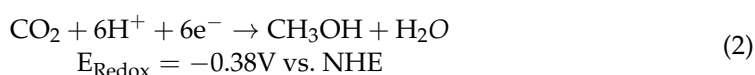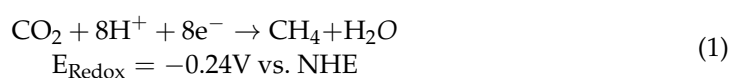

Figure 3. Kinetics of CO_2 photoinduced conversion in gas phase under illumination UV-A (370 nm): to methane (**a**), to methanol (**b**).

Only two compounds increased in concentration in the presence of CO_2 flux: methane and methanol. This is evidence of photoinduced CO_2 conversion. One can see that maximum methanol outcome was observed for the SW TiO_2 NTs sample while minimum methane output was observed for this sample. Deposition of copper oxide shifts the selectivity of the conversion process to methane production. Output of methane reaches its maximum for the SW TiO_2 NTs/CuxO-30 sample. Increasing the number of deposition cycles from 10 to 60 led to an increase in methanol output. However, the rate of methanol production for the samples with deposited copper oxide remains smaller than for the SW TiO_2 NTs sample.

Variation of CO_2 conversion selectivity can be explained by the difference of methane and methanol formation potentials and changing of conduction band potentials of TiO_2 in contact with CuO. Potentials of reactions of methane (1) and methanol (2) formations are equal to -0.24 V and -0.38 V versus normal hydrogen electrode (NHE), respectively [36].

$$CO_2 + 8H^+ + 8e^- \rightarrow CH_4 + H_2O$$
$$E_{Redox} = -0.24V \text{ vs. NHE} \tag{1}$$

$$CO_2 + 6H^+ + 6e^- \rightarrow CH_3OH + H_2O$$
$$E_{Redox} = -0.38V \text{ vs. NHE} \tag{2}$$

According to photoelectrochemical data, the conduction band bottom potential in TiO_2 is more negative compared to methanol reaction potential [37]. Therefore, reactions (1) and (2) can take place at the surface of TiO_2. Redistribution of charge carriers between two semiconductors occurs after deposition of copper oxide on the surface of anodic titania nanotube arrays. This leads to the bending of energy bands in semiconductors (Figure 4). The band edges positions of copper oxides are indicated according data in the literature [18,33,38].
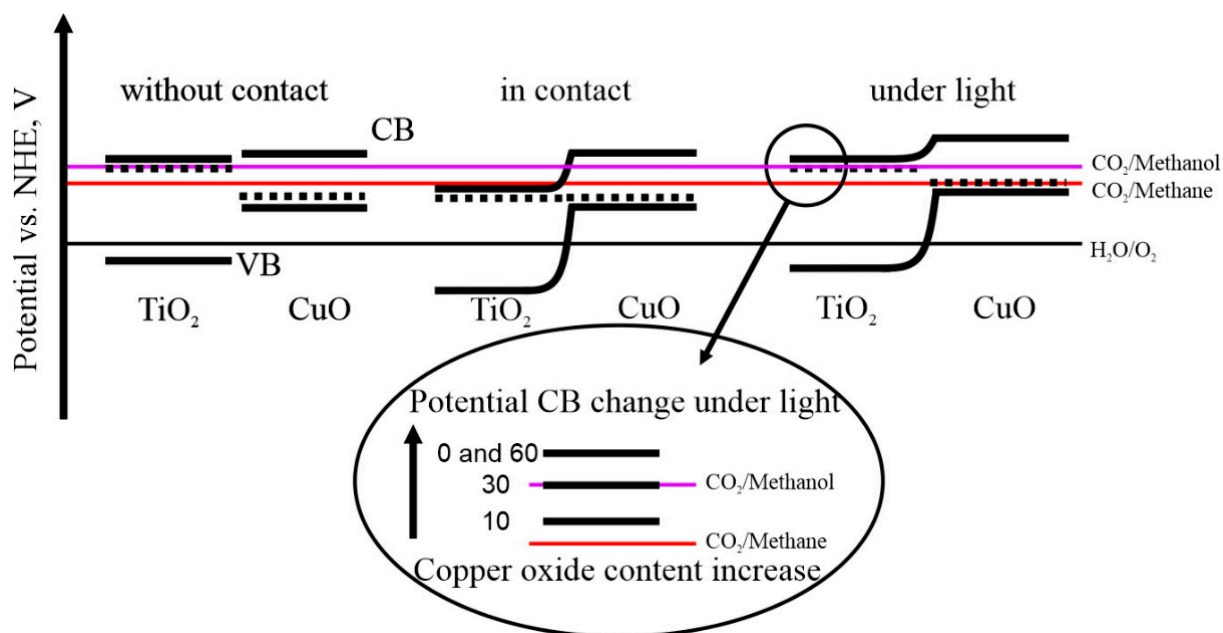

Figure 4. Energy band bending model in NTs/Cu$_x$O composites.

As a result of the band-bending, the conduction band potential in TiO_2 becomes more positive than the reduction potential for the reaction (2). The latter can block the reaction. Illumination, in turn, shifts energy band potentials in TiO_2 to more negative values due to the migration of photoelectrons from CuO to TiO_2. This can lead to an increased probability of the reaction occurring (2). Variation (increase) of an amount of copper oxide leads in

turn to the enhancement of the concentration of photogenerated charge carriers and thus to more significant flattening of energy band in TiO_2.

This mechanism makes the shift of CO_2 photoconversion selectivity towards methane production, caused by deposition of copper oxide on TiO_2 NTs arrays, understandable. One can suggest that the conduction band potential of TiO_2 in NTs/Cu_xO-10 sample is appropriate for CO_2 photoconversion to methane but not to methanol. For the NTs/Cu_xO-30 sample, the conduction band potential is also not negative enough for the reaction (2). However, methane output increases due to larger photoelectron concentration separated at the heterojunction of two semiconductors. Deposition of a larger amount of copper oxide (NTs/Cu_xO-60 sample) makes band flattening under illumination large enough for the reaction (2). However, efficiency of methanol production for this sample is smaller than for non-modified sample SW TiO_2 NTs. This fact can be linked to the impossibility of water decomposition on the surface of copper oxide due to insufficient positive potential of the top of valence band. As a consequence, hydrogen ions and hydroxyl ions can be formed only on the surface of TiO_2. The free surface of TiO_2 of NTs decreases with an increase in the amount of copper oxide deposition cycles resulting in a reduction in the rate of CO_2 photoconversion to methanol.

2.4. Electron Paramagnetic Resonance

The nanocomposites obtained were further investigated by electron paramagnetic resonance spectroscopy (EPR) since defects (spin centers) play an important role in photocatalytic processes [6]. The main type of defect in initial SW TiO_2 NTs is Ti^{3+}/oxygen vacancy (g_1 = 1.9961, g_2 = 1.9697). Figure 5a shows the EPR spectra of SW TiO_2 NTs in the dark and under illumination. It can be seen (Figure 5a) that, upon photoexcitation, the intensity of the EPR signal (I_{EPR}) increases slightly.
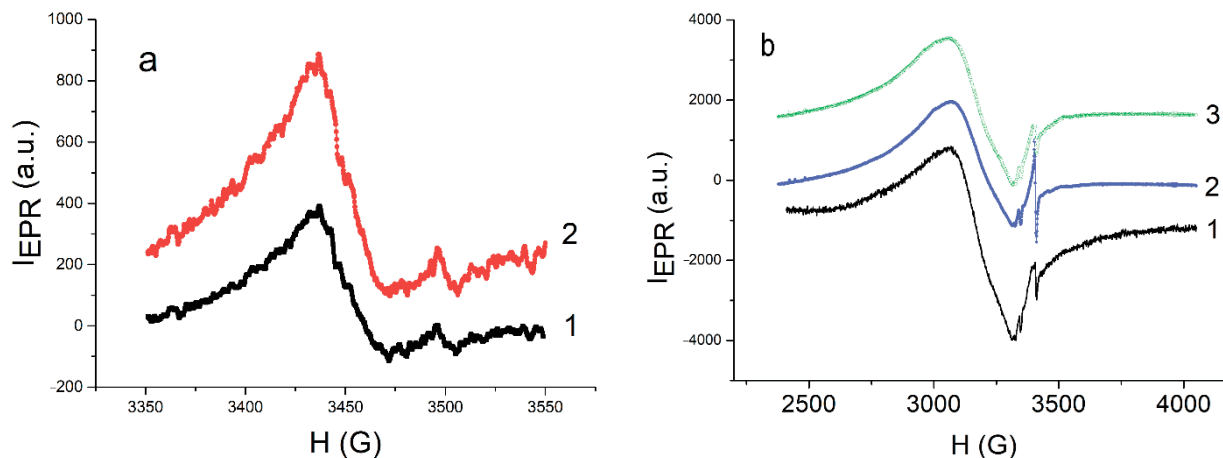

Figure 5. (**a**) EPR spectra of SW TiO_2 NTs in dark (1) and under illumination (2). (**b**) EPR spectra of SW TiO_2 NTs/Cu_xO-30 in dark (1), under illumination (2) and in dark after illumination (3).

Figure 5b shows an example of the EPR spectrum of the SW TiO_2 NTs/Cu_xO-30 nanocomposites. This spectrum is a superposition of several EPR signals. First, a strong EPR signal from copper ions Cu^{2+} (g = 2.1612) [39] is detected (Figure 5b), which indicates the presence of the CuO phase. We also observed on the right side of the EPR spectrum the signal from O_2^- radicals (g_1 = 2.029, g_2 = 2.009, g_3 = 2.003). The appearance of O_2^- radicals can be explained by the adsorption of oxygen molecules on oxygen vacancies on the surface of TiO_2 and, probably, on the surface of copper oxide nanoparticles, followed by the capture of electrons from the conduction band. Upon illumination, the EPR signal intensity from Cu^{2+} decreases while EPR signal intensity from O_2^- radicals increases (Figure 5b). We suppose that paramagnetic defects Cu^{2+} pass into a non-paramagnetic state ($Cu^{2+} + e^- \rightarrow Cu^+$), which leads to a diminution of corresponding EPR signal (Figure 5b).

At the same time, the capture of a photoinduced electron by an oxygen molecule leads to an increase in the EPR signal from O_2^- radicals: $O_2 + e^- \rightarrow O_2^-$. The generation of Cu^+ ions under illumination indicates the formation of Cu_2O phase.

Notice that we did not observe the EPR signal in SW TiO_2 NTs/Cu_xO nanocomposites from the Ti^{3+}/oxygen vacancy centers, probably against the background of strong EPR signals from copper ions and oxygen radicals. Under illumination, they are also not recorded, as these defects probably capture the photoexcited hole and pass into a non-paramagnetic state: $Ti^{3+} + h \rightarrow Ti^{4+}$. Therefore, in SW TiO_2 NTs/Cu_xO nanocomposites the defects accumulate the charge necessary for redox reactions. We also investigated the behavior of spin centers after illumination. Figure 5b shows EPR spectrum of SW TiO_2 NTs/Cu_xO-30 one hour after illumination (spectrum 3). It can be seen that the EPR signal intensity from Cu^{2+} increases a little but does not reach the value before illumination, while EPR signal intensity from O_2^- radicals strongly decreases to the value before illumination. Therefore, a phase transformation of CuO to Cu_2O takes place during illumination. A reduction of O_2^- radicals after illumination can be due to spending radicals in redox reactions.

2.5. Secondary Ion Mass Spectroscopy

To understand the nature of copper oxide alternation on TiO_2 surface, two parts of the same sample were studied before and after illumination by means of secondary ion mass spectroscopy (SIMS).

It has been found that emission of CuO^- and CuO^{2-} (normalized to total amount of detected ions) is much higher from the sample before illumination compared to emission after illumination. Moreover, there is a difference in the ratio of amount of emitted CuO^{2-} and CuO^- ions before and after illumination. This difference can point to the different stoichiometry of copper oxides on the surface of the samples before and after illumination. One can suggest that the amount of oxygen bound to copper is larger before illumination. The data obtained provide evidence to suggest that copper oxide on the surface of the samples is most likely in the CuO phase before illumination. However, after illumination, copper oxide transforms to a less oxidized Cu_2O phase, which is consistent with the EPR data. We suppose that copper oxide operates as a source of photogenerated electrons. Their quantity controls potentials of energy bands in TiO_2.

2.6. Role of Cu_2O in Photocatalytic Conversion of CO_2

Taking into account transformation of CuO to Cu_2O phase, one can present an energy diagram of the structure as an energy diagram of heterostructure consisting of three semiconductors. Transformation of CuO to Cu_2O can take place at the TiO_2/CuO boundary and at CuO free surface (Figure 6). The change of copper oxide phase will not lead to significant shift of Fermi level position due to the small amount of Cu_2O formed compared to the amount of titania. For both possible positions of Cu_2O phase shown in Figure N, the amount of photoelectrons transferred to TiO_2 will be reduced due to their additional recombination at the CuO/Cu_2O boundary or accumulation in the CuO phase followed by CuO transformation to Cu_2O and to Cu [32]. Therefore, elevating of Fermi level caused by illumination will be smaller in the structure containing Cu_2O than in the structure with CuO phase only. Thus, the probability of methanol formation should be reduced due to CuO to Cu_2O phase transformation. The probability of methane formation can also be reduced but less significantly due to the less negative potential of methane formation.

Based on the data obtained, one can suggest that the efficiency and selectivity of CO_2 conversion in the Cu_2O-CuO-TiO_2 system is determined by the number of photoelectrons transferred to TiO_2. This number determines the rise of Fermi level in TiO_2 under illumination and its position with respect to potentials for CO_2 to methane or methanol conversion. At high concentrations of photoelectrons, the position of the Fermi level under illumination is high enough for effective conversion of CO_2 to methanol (2). At lower concentrations of

photoelectrons, the position of the Fermi level is too low for effective methanol production. In this case, methane production (1) dominates.
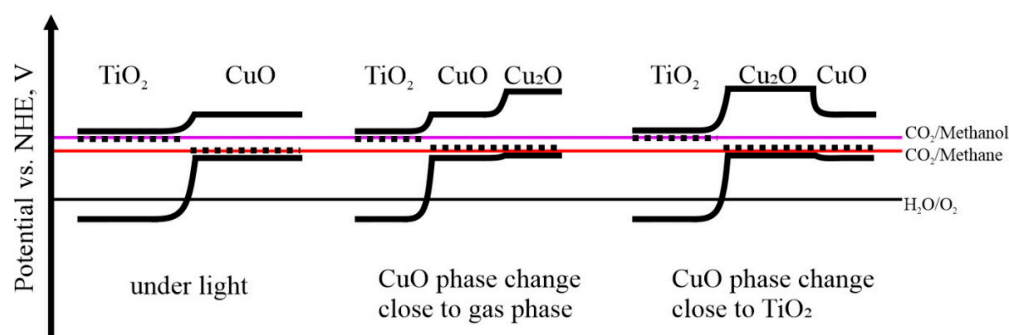

Figure 6. Energy band bending model in NTs/CuO-Cu$_2$O composites.

3. Materials and Methods

Synthesis of single-wall (SW) nanotubes of anodic titania is described in [34]. SW TiO$_2$ NTs/Cu$_x$O nanocomposites were prepared by deposition of copper oxide on the surface of titania nanotubes arrays using successive ionic layer adsorption and reaction (SILAR). An aqueous solution of CuCl$_2$·2H$_2$O served as ionic source. An aqueous solution of 25% NH$_4$OH (Russian Specifications GOST 3760-79, Sigma Tec, Khimki, Russia) was added to increase the pH to 10. Mixture of ethanol with deionized water in 1:3 proportion heated up to 70 °C was used as the source of anions. The SILAR method was carried out in three stages. In the first stage, the sample was inserted into an aqueous solution of copper chloride containing [Cu(NH$_3$)$_4$]$^{2+}$ ions for 30 s. In the second stage, the sample was inserted into a mixture of ethanol with deionized water for 7 s. In the third stage, the sample washed in deionized water for 30 s.

Variation of the amount of copper oxide Cu$_x$O deposited on SW TiO$_2$ NTs was performed by variation of cycles of ionic layer formation (10, 30 and 60 cycles were carried out for samples SW TiO$_2$ NTs/Cu$_x$O-10, SW TiO$_2$ NTs/Cu$_x$O-30 and SW TiO$_2$ NTs/Cu$_x$O-60, respectively). After deposition, the samples were heated up to 300 °C at a rate of 30 °C/min and kept at 300 °C in air for 60 min.

The surface morphologies and compositions were studied using a Helios G4CX (Thermo Fisher Scientific, Waltham, MA, USA) scanning electron microscope equipped with an EDS attachment (EDAX Octane Elite Super).

Spectra of diffuse light reflection from SW TiO$_2$ NTs and SW TiO$_2$ NTs/Cu$_x$O samples were recorded on LS-55 Perkin Elmer spectrometer (Waltham, MA, USA) which allows for the registration of the diffuse light scattering from the sample surface in a spectral range from 200 to 800 nm with spectral slit widths from 2.5 to 20 nm.

Electron paramagnetic resonance (EPR) spectra were recorded on a Bruker ELEXSYS E500 EPR spectrometer (Billerica, MA, USA) (X-band). The samples were illuminated directly in the cavity of the EPR spectrometer with the light of a BRUKER ELEXSYS ER 202 UV high-pressure mercury lamp (50 W). The photoexcitation intensity of the samples was 40 mW/cm^2.

Secondary ion mass spectroscopy was produced by TOF-SIMS IV manufactured by IONTOF GmbH, Muenster, Germany, and clusters of bismuth ion (Bi^{3+}) were used.

The details of the methodology of the photocatalytic conversion of CO$_2$ were presented earlier in the work [34]. The photocatalytic CO$_2$ conversion was provided under the following conditions: reactor temperature 30 °C, relative humidity 5%, total CO$_2$ (ISO 14175-C1) gas flow 1.2 mL/min. The analysis of the gas products was carried out using an HP PLOT/Q capillary column Hewlett Packard HP 5890 Series II Gas Chromatograph-FID (Agilent Technologies, Santa Clara, CA, USA).

4. Conclusions

Single-walled TiO_2 nanotube-Cu_xO composites for converting carbon dioxide (CO_2) into hydrocarbon compounds were prepared. Methanol and methane were detected during the CO_2 photoreduction process. The production rate of gas-phase CO_2 conversion and photoinduced transformations of defects in the prepared photocatalysts were investigated. Only Ti^{3+}/oxygen vacancy defects were detected by EPR spectroscopy in initial TiO_2 nanotubes. Cu^{2+} centers and O_2^- radicals were detected in the TiO_2 nanotube–Cu_xO composites. Under illumination, the capture of a photoinduced electron by oxygen molecules led to an increase in the EPR signal from O_2^- radicals. It was shown by EPR technique that Cu_xO nanoparticles are present in the TiO_2 nanotube-Cu_xO composites in the form of the CuO phase. Under illumination, a phase transformation of CuO to Cu_2O was observed. These results are consistent with data obtained by secondary ion mass spectroscopy. The shift of CO_2 photoconversion selectivity was observed towards methane production due to the deposition of copper oxide on the surface of TiO_2 nanotubes. The mechanism of methane and methanol formation in the TiO_2 nanotubes with different copper oxide content is discussed. The obtained results are completely novel and show a high level of importance for the development of energy-efficient photocatalysts for CO_2 conversion into hydrocarbon fuel precursors.

References

1. Smith, P.; Davis, S.J.; Creutzig, F.; Fuss, S.; Minx, J.; Gabrielle, B.; Kato, E.; Jackson, R.B.; Cowie, A.; Kriegler, E.; et al. Biophysical and economic limits to negative CO_2 emissions. *Nat. Clim. Change* **2016**, *6*, 42–50. [CrossRef]
2. Vijaya, V.; Raman, S.; Iniyan, S.; Goic, R. A review of climate change, mitigation and adaptation. *Renew. Sustain. Energy Rev.* **2012**, *16*, 878–897.
3. Saravanan, A.; Senthil Kumar, P.; Dai-Viet, N.V.; Jeevanantham, S.; Bhuvaneswari, V.; Anantha, N.V.; Yaashikaa, P.R.; Swetha, S.; Reshma, B. A comprehensive review on different approaches for CO_2 utilization and conversion pathways. *Chem. Eng. Sci.* **2021**, *236*, 116515. [CrossRef]
4. Kovacič, Ž.; Likozar, B.; Hus, M. Photocatalytic CO_2 Reduction: A Review of Ab Initio Mechanism, Kinetics, and Multiscale Modeling Simulations. *ACS Catal.* **2021**, *10*, 14984–15007. [CrossRef]
5. Sorcar, S.; Hwang, Y.; Lee, J.; Kim, H.; Grimes, K.M.; Grimes, C.A.; Jung, J.-W.; Cho, C.-H.; Majima, T.; Hoffmann, M.R.; et al. CO_2, water, and sunlight to hydrocarbon fuels: A sustained sunlight to fuel (Joule-to-Joule) photoconversion efficiency of 1%. *Energy Environ. Sci.* **2019**, *12*, 2685–2696. [CrossRef]
6. Rawool, S.A.; Yadav, K.K.; Polshettiwar, V. Defective TiO_2 for photocatalytic CO_2 conversion to fuels and chemicals. *Chem. Sci.* **2021**, *12*, 4267–4269. [CrossRef] [PubMed]

7.　Zubair, M.; Kim, H.; Razzaq, A.; Grimes, C.A.; In, S.-I. Solar spectrum photocatalytic conversion of CO_2 to CH_4 utilizing TiO_2 nanotube arrays embedded with graphene quantum dots. *J. CO_2 Util.* **2018**, *26*, 70–79. [CrossRef]

8.　Liu, Z.; Zhang, X.; Nishimoto, S.; Murakami, T.; Fujishima, A. Efficient Photocatalytic Degradation of Gaseous Acetaldehyde by Highly Ordered TiO_2 Nanotube Arrays. *Environ. Sci. Technol.* **2008**, *42*, 8547–8551. [CrossRef]

9.　Low, J.; Qiu, S.; Xu, D.; Jiang, C.; Cheng, B. Direct evidence and enhancement of surface plasmon resonance effect on Ag-loaded TiO_2 nanotube arrays for photocatalytic CO_2 reduction. *Appl. Surf. Sci.* **2018**, *434*, 423–432. [CrossRef]

10.　Varghese, O.K.; Paulose, M.; LaTempa, T.J.; Grimes, C.A. High-Rate Solar Photocatalytic Conversion of CO_2 and Water Vapor to Hydrocarbon Fuels. *Nano Lett.* **2009**, *9*, 731–737. [CrossRef]

11.　Liu, N.; Mirabolghasemi, H.; Lee, K.; Albu, S.P.; Tighineanu, A.; Altomare, M.; Schmuki, P. Anodic TiO_2 nanotubes: Double walled vs. single walled. *Faraday Discuss.* **2013**, *164*, 107. [CrossRef] [PubMed]

12.　Belov, A.N.; Gavrilin, I.M.; Gavrilov, S.A.; Dronov, A.A.; Labunov, V. Effect of the activity of fluorine-containing electrolytes on reaching the maximum thickness of porous anodic titanium oxide. *Semiconductors* **2013**, *47*, 1707–1710. [CrossRef]

13.　So, S.; Riboni, F.; IHwang Paul, D.; Hammond, J.; Tomanec, O.; Zboril, R.; Sadoway, D.R.; Schmuki, P. The double-walled nature of TiO_2 nanotubes and formation of tube-in-tube structures—A characterization of different tube morphologies. *Electrochim. Acta* **2017**, *231*, 721–731. [CrossRef]

14.　Dronov, A.; Gavrilin, I.; Kirilenko, E.; Dronova, D.; Gavrilov, S. Investigation of anodic TiO_2 nanotube composition with high spatial resolution AES and ToF SIMS. *Appl. Surf. Sci.* **2018**, *434*, 148–154. [CrossRef]

15.　Gavrilin, I.; Dronov, A.; Volkov, R.; Savchuk, T.; Dronova, D.; Borgardt, N.; Pavlikov, A.; Gavrilov, S.; Gromov, D. Differences in the local structure and composition of anodic TiO_2 nanotubes annealed in vacuum and air. *Appl. Surf. Sci.* **2020**, *516*, 146120. [CrossRef]

16.　Motola, M.; Sopha, H.; Krbal, M.; Hromádko, L.; Zmrhalová, Z.O.; Plesch, G.; Macak, J.M. Comparison of photoelectrochemical performance of anodic single- and double-walled TiO_2 nanotube layers. *Electrochem. Commun.* **2018**, *97*, 1–5. [CrossRef]

17.　Xi, H.; Xu, Y.; Zou, W.; Ji, J.; Cai, Y.; Wan, H.; Dong, L. Enhanced methanol selectivity of Cu_xO/TiO_2 photocatalytic CO_2 reduction: Synergistic mechanism of surface hydroxyl and low-valence copper species. *J. CO_2 Util.* **2022**, *55*, 101825. [CrossRef]

18.　Park, S.-M.; Razzaq, A.; Park, Y.H.; Sorcar, S.; Park, Y.; Grimes, C.A.; In, S.-I. Hybrid Cu_xO-TiO_2 Heterostructured Composites for Photocatalytic CO_2 Reduction into Methane Using Solar Irradiation: Sunlight into Fuel. *ACS Omega* **2016**, *1*, 868–875. [CrossRef]

19.　Miyauchi, M.; Sunada, K.; Hashimoto, K. Antiviral Effect of Visible Light-Sensitive Cu_xO/TiO_2 Photocatalyst. *Catalysts* **2020**, *10*, 1093. [CrossRef]

20.　Bharad, P.A.; Nikam, A.V.; Thomas, F.; Gopinath, C.S. CuO_x-TiO_2 Composites: Electronically Integrated Nanocomposites for Solar Hydrogen Generation. *Chem. Sel.* **2018**, *3*, 12022–12030.

21.　Wang, K.; Bielan, Z.; Endo-Kimura, M.; Janczarek, M.; Zhang, D.; Kowalski, D.; Zielińska-Jurek, A.; Markowska-Szczupak, A.; Ohtani, B.; Kowalska, E. On the mechanism of photocatalytic reactions on $Cu_xO@TiO_2$ core–shell photocatalysts. *J. Mater. Chem. A* **2021**, *9*, 10135–10145. [CrossRef]

22.　Saedy, S.; Hiemstra, N.; Benz, D.; Bui, H.V.; Nolan, M.; van Ommen, J.R. Dual promotional effect of Cu_xO clusters grown with atomic layer deposition on TiO_2 for photocatalytic hydrogen production. *Catal. Sci. Technol.* **2022**. *12*, 4511–4523. [CrossRef]

23.　Li, H.; Zhou, J.; Feng, B. Facile synthesis of Cu_xO (x = 1, 2)/TiO_2 nanotube arrays as an efficient visible-light driven photocatalysts. *J. Porous Mater.* **2017**, *24*, 97–102. [CrossRef]

24.　Srivinas, B.; Shubhamangala, B.; Lalitha, K.; Kumar Reddy, P.A.; Kumari, V.D.; Subrahmanyam, M.; De, B.R. Photocatalytic Reduction of CO_2 over $Cu-TiO_2$/Molecular Sieve 5A Composite. *Photochem. Photobiol.* **2011**, *87*, 995–1001.

25.　Liu, C.; Iyemperumal, S.K.; Deskins, N.A.; Li, G. Photocatalytic CO_2 Reduction by Highly Dispersed Cu Sites on TiO_2. *J. Photonics Energy* **2016**, *7*, 012004. [CrossRef]

26.　Méndez-Medrano, M.G.; Kowalska, E.; Ohtani, B.; Bahena Uribe, D.; Colbeau-Justin, C.; Rau, S.; Rodríguez-López, J.L.; Remita, H. Heterojunction of CuO Nanoclusters with TiO_2 for Photo-Oxidation of Organic Compounds and for Hydrogen Production. *J. Chem. Phys.* **2020**, *153*, 034705. [CrossRef] [PubMed]

27.　Janczarek, M.; Kowalska, E. On the Origin of Enhanced Photocatalytic Activity of Copper-Modified Titania in the Oxidative Reaction Systems. *Catalysts* **2017**, *7*, 317. [CrossRef]

28.　Hamad, H.; Elsenety, M.M.; Sadik, W.; El-Demerdash, A.G.; Nashed, A.; Mostafa, A.; Elyamny, S. The Superior Photocatalytic Performance and DFT Insights of S-Scheme $CuO@TiO_2$ Heterojunction Composites for Simultaneous Degradation of Organics. *Sci. Rep.* **2022**, *12*, 317. [CrossRef]

29.　Shi, Q.; Ping, G.; Wang, X.; Xu, H.; Li, J.; Cui, J.; Abroshan, H.; Ding, H.; Li, G. CuO/TiO_2 Heterojunction Composites: An Efficient Photocatalyst for Selective Oxidation of Methanol to Methyl Formate. *J. Mater. Chem. A* **2019**, *7*, 2253–2260. [CrossRef]

30.　Aguirre, M.E.; Zhou, R.; Eugene, A.J.; Guzman, M.I.; Grela, M.A. Cu_2O/TiO_2 Heterostructures for CO_2 Reduction through a Direct Z-Scheme: Protecting Cu_2O from Photocorrosion. *Appl. Catal. B Environ.* **2017**, *217*, 485–493. [CrossRef]

31.　Rehman, Z.U.; Bilal, M.; Hou, J.; Butt, F.K.; Ahmad, J.; Ali, S.; Hussain, A. Photocatalytic CO_2 Reduction Using TiO_2-Based Photocatalysts and TiO_2 Z-Scheme Heterojunction Composites: A Review. *Molecules* **2022**, *27*, 2069. [CrossRef] [PubMed]

32.　De Almeida, J.; Pacheco, M.S.; de Brito, J.F.; de Arruda Rodrigues, C. Contribution of Cu_xO Distribution, Shape and Ratio on TiO_2 Nanotubes to Improve Methanol Production from CO_2 Photoelectroreduction. *J. Solid State Electrochem.* **2020**, *24*, 3013–3028. [CrossRef]

33. Li, Y.; Zhang, W.; Shen, X.; Peng, P.; Xiong, L.; Yu, Y. Octahedral Cu_2O-modified TiO_2 nanotube arrays for efficient photocatalytic reduction of CO_2. *Chin. J. Catal.* **2015**, *36*, 2229–2236. [CrossRef]

34. Savchuk, T.; Gavrilin, I.; Konstantinova, E.; Dronov, A.; Volkov, R.; Borgardt, N.; Maniecki, T.; Gavrilov, S.; Zaitsev, V. Anodic TiO_2 nanotube arrays for photocatalytic CO_2 conversion: Comparative photocatalysis and EPR study. *Nanotechnology* **2022**, *33*, 055706. [CrossRef] [PubMed]

35. Sviridova, T.V.; Sadovskaya LYu Konstantinova, E.A.; Belyasova, N.A.; Kokorin, A.I.; Sviridov, D.V. Photoaccumulating TiO_2–MoO_3, TiO_2–V_2O_5, and TiO_2–WO_3 Heterostructures for Self-Sterilizing Systems with the Prolonged Bactericidal Activity. *Catal. Lett.* **2019**, *149*, 1147–1153. [CrossRef]

36. Abdullah, H.; Khan, M.M.R.; Ong, H.R.; Yaakob, Z. Modified TiO_2 Photocatalyst for CO_2 Photocatalytic Reduction: An Overview. *J. CO_2 Util.* **2017**, *22*, 15–32. [CrossRef]

37. Ola, O.; Maroto-Valer, M.M. Review of Material Design and Reactor Engineering on TiO_2 Photocatalysis for CO_2 Reduction. *J. Photochem. Photobiol. C Photochem. Rev.* **2015**, *24*, 16–42. [CrossRef]

38. Tan, Y.; Wei, Y.; Xu, Y.; Liang, K.; Jiao, Y.; Zhang, S. A Novel Nano-Pore Stainless Steel Film Modified by $Cu@CuO/Cu_2O$ Semiconductor Heterojunction for Photoelectrocatalytic Activity and Semiconductor Characteristics. *ECS J. Solid State Sci. Technol.* **2021**, *10*, 063002. [CrossRef]

39. Martín-Gomez, J.; Hidalgo-Carrillo, J.; Montes, V.; Estevez-Toledano, R.C.; Escamilla, J.C.; Marinas, A.; Urbano, F.J. EPR and CV studies cast further light on the origin of the enhanced hydrogen production through glycerol photoreforming on $CuO:TiO_2$ physical mixtures. *J. Environ. Chem. Eng.* **2021**, *9*, 105336. [CrossRef]